RSC Advances

High rate capabilities of Li4Ti5-xVxO12 (0 ≤ x ≤ 0.3) anode materials prepared by sol-gel method for power lithium ion battery

Journal:	*RSC Advances*
Manuscript ID:	RA-ART-02-2015-003549.R1
Article Type:	Paper
Date Submitted by the Author:	11-May-2015
Complete List of Authors:	Chang, Chien-Min; Chung Yuan Christian University, Chemistry Chen, Yi-Chih; Chung Yuan Christian University, Chemistry Ma, Wei-Lun; Chung Yuan Christian University, Chemistry Chen, yuiwhei; Chung Yuan Christian University, Chemistry

Graphical Abstract

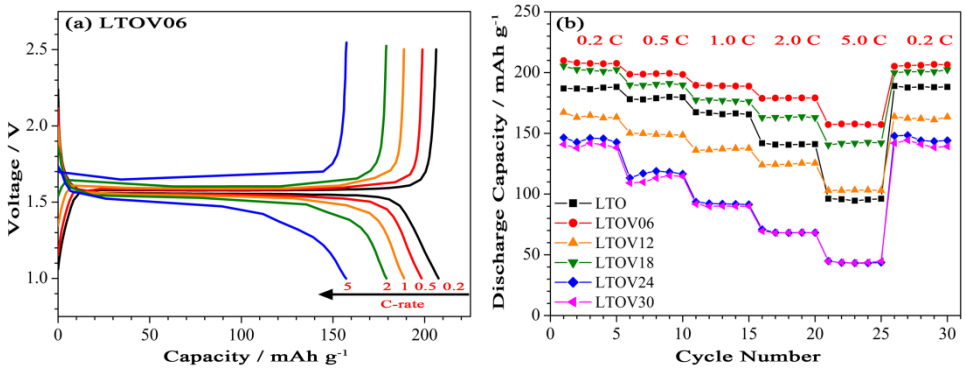

(a) Charge-discharge curves of the LTOV06 electrode at various rates. (b) The rate capabilities of the $Li_4Ti_{5-x}V_xO_{12}$ ($0 \leq x \leq 0.3$) electrodes at various rates in 1 - 2.5 V for coin half-cell. The results show that the highest capacities, 208 (0.2 C), 198 (0.5 C), 189 (1 C), 179 (2 C), 157 mAh g^{-1} (5 C), are obtained from the LTOV06 electrode, which are higher than those of the LTO electrodes reported.

Journal Name

RSCPublishing

ARTICLE

High rate capabilities of $Li_4Ti_{5-x}V_xO_{12}$ ($0 \le x \le 0.3$) anode materials prepared by sol-gel method for power lithium ion battery

Cite this: DOI: 10.1039/x0xx00000x

Received 00th January 2012,
Accepted 00th January 2012

DOI: 10.1039/x0xx00000x

www.rsc.org/

Chien-Min Chang[a], Yi-Chih Chen[a], Wei-Lun Ma[a], Yui Whei Chen-Yang[a,b,c*]

In this study, the spinel-type vanadium-doped $Li_4Ti_{5-x}V_xO_{12}$ ($0 \le x \le 0.3$) samples (LTOVs) are synthesized by the sol-gel method. It is found that the LTOVs are formed with the nano-particles of 5 - 15 nm in diameter. The V-doping does not cause any phase change in its structure and barely affects the lattice parameter, while varies the ratio of Ti^{3+} and Ti^{4+} oxidation states. The electrochemical analyses demonstrate that the best discharge capacities are obtained from the $Li_4Ti_{5-x}V_xO_{12}$ (x = 0.06) electrode (LTOV06 electrode) in the voltage range of 1 - 2.5 V at 0.2, 0.5, 1, 2 and 5 C with 208, 198, 189, 179 and 157 mAh g^{-1}, respectively. At 1 C the discharge capacity remains at 186 mAh g^{-1} after 50 cycles, keeping good cyclic performance. Besides, in the voltage range of 0 - 2.5 V at 5 C, the initial discharge capacity of the LTOV06 electrode is at 243 mAh g^{-1} and retains 89 % after 250 cycles. The results indicate that LTOV06 is a promising high-rate anode material for lithium ion batteries.

1. Introduction

Recently, the research focus of rechargeable lithium ion battery (LIB) in application has been transferred from energy battery to power battery because its high power density and high-rate capability can meet the requirement of the application in electric vehicles (EVs), hybrid electric vehicles (HEVs) and other load-leveling applications.[1, 2] Nevertheless, the safety issues of LIB are always concerned especially for the large batteries.[3] Compared to the currently used carbonaceous materials such as graphite, the spinel-type $Li_4Ti_5O_{12}$ (LTO) has been regarded as the potential materials of the next generation anode due to the negligible change of volume during electrochemical cycling and the high redox platforms at around 1.55 V *vs.* Li/Li^+, avoiding the reduction of electrolyte.[4, 5] Although LTO is more stable and safer than the carbonaceous materials, its poor electronic conductivity, leading to a lower specific capacity, is the disadvantage to be improved.[6] Hence, the methods, such as reducing particle size, coating with carbon or metallic conducting layer and doping with metal ions, have been reported to enhance the conductivity and rate capability of LTO.[7-10] For the metal ion-doped LTO (LTOM), the increase in electronic conductivity was ascribed to the generation of some Ti^{3+} by charge compensation.[11] Table 1 lists the electrochemical cycling data of the LTOMs with various doping metal ions in the Ti site.[6, 11-22] As can be seen, most of the LTOM electrode materials were prepared with solid state method. This is because it is a convenient and low cost process, having the commercial application potential. On the other hand, although few LTOMs prepared with sol-gel method were reported, it was found that the sol-gel method was not only able to dope the metal ions in the spinel structure but also produce nano-particles, leading to the better electrochemical properties.[23] Especially, the Nb-doped $Li_4Ti_{5-x}Nb_xO_{12}$ (x = 0.05) prepared with sol-gel method by Wang et al.[6] exhibited a high discharge capacity of 179 mAh g^{-1} at 0.5 C and an initial capacity of 145 mAh g^{-1} at 10 C with a capacity of 116 mAh g^{-1} at the 100th cycle. Nevertheless, the Nb is relatively expensive and rare on earth. On the other hand, vanadium was considered to be a cheaper and more abundant metal than Nb. Yi et al.[21, 22] prepared a series of V-doped LTOs, $Li_4Ti_{5-x}V_xO_{12}$ ($0 \le x \le 0.3$), with solid state method and obtained good capacities for $Li_4Ti_{5-x}V_xO_{12}$ (x = 0.05). However, the high rate capacities were not studied. Wang et al.[11] used high-speed ball milled method to down size the $Li_4Ti_{5-x}V_xO_{12}$ (x = 0.1) particles and found that the reduction of the particle size did improve the electrochemical properties. Yet, the capacity was still no better than that of Nb-doped LTO mentioned above, possibly because the particle size was not smaller enough. These results revealed that synthesis of a high-rate performance anode material with a good combination of cheaper metal doper and proper method, such as V-doped LTO and sol-gel method is still worth to pursuit. Although $Li_{4.25}Ti_{4.75}V_{0.25}O_{12}$ with sol-gel method had been prepared by Jumas,[24] its discharge capacity was only 74 mAh g^{-1} at less than 0.1 C, and the rate capability was not reported. Since the product of sol-gel process depends on the precursor, temperature, calcination condition etc., in this study, we synthesized a series of the vanadium-doped $Li_4Ti_{5-x}V_xO_{12}$ (x = 0.00 - 0.30) (LTOVs) by the sol-gel process under a proper condition and studied their electrochemical properties. Moreover, the oxidation states of titanium and vanadium and morphologies of the as-prepared LTOV materials were examined in detail to study the loading effect of V-doping at the high-rate and the cycle stability of the LTOVs in the voltage range of 1 - 2.5 V and 0 - 2.5 V *vs.* Li/Li^+.

Table 1 Summary of electrochemical cycling data of $Li_4Ti_5O_{12}$ with different doping metal ions in the Ti site

Doping Metal ions $Li_4Ti_{5-x}M_xO_{12}$		Preparation method	The capacities in the voltage range of 1 - 2.5 V				Ref.
			AM[a] (%)	Reversible capacity at C-rate (mAh g^{-1} @ C)		Cyclic performance Capacity value; after "n" cycles	
M = Al,	x = 0.05	Sol-gel	83	169 @ 0.1 C;	116 @ 5 C	110 @ 5 C; 50	12
M = Al,	x = 0.05	Solid state	80	227 @ 0.2 C		160 @ 0.2C; 50	13
M = Al,	x = 0.15	Cellulose combustion	85	212 @ 1 C;	180 @ 5C	Capacity retention 95% @ 5C; 50	14
M = Al,	x = 0.15	Solid state	80	196[b] @ 0.15 mA cm^{-2}		167[b] @ 0.15 mA cm^{-2}; 30	15
M = Zr,	x = 0.1	Solid state	85	159 @ 0.5 C;	151 @ 1 C	143 @ 5 C; 100	16
M = Nb,	x = 0.05	Sol-gel	82	179 @ 0.5 C;	145 @ 10 C; 82 @ 40 C	116 @ 10 C; 100	6
M =Mo,	x = 0.1	Solid state	80	276[c] @ 0.1 C;	243[c] @ 6 C	211[c] @ 6 C; 100	17
M = Ru,	x = 0.05	Solid state	80	233[c] @ 1 C;	154[c] @ 10 C	132[c] @ 10 C; 100	18
M = La,	x = 0.05	Solid state	82	~220[c] @ 0.5 C;	201[c] @ 5 C	181[c] @ 5 C; 200	19
M = Ni and Mn,	x = 0.10	Sol-gel	85	172 @ 0.5 C		143 @ 0.5 C; 100	20
M = V,	x = 0.05	Solid state	82	171 @ 0.1 C		157 @ 0.1 C; 110	21
M = V,	x = 0.05	Solid state	80	Higher than theoretical capacity (298)[c] @ 0.2 C		218[c] @ 0.2 C; 50	22
M = V,	x = 0.1	High-speed ball milled	80	178 @ 0.1 C;	114 @ 5 C	Capacity retention 93% @ 5C; 4374	11
M = V,	x = 0.06	Sol-gel	80	208 @ 0.2 C;	157 @ 5 C	186 @ 1 C; 50 243[c] @ 5 C; 250	**This work**

[a] The weight percentage of active material in the electrode

[b]The capacity in the voltage range of 0.5 - 2.5 V

[c]The capacity in the voltage range of 0 - 2.5 V

2. Experimental

2.1. Materials Preparation

The spinel-type oxide with nominal compositions of $Li_4Ti_{5-x}V_xO_{12}$ (x = 0, 0.06, 0.12, 0.18, 0.24, 0.30) were synthesized by sol-gel method from the mixture of lithium acetate (CH_3COOLi, Alfa Aesar), vanadium oxide (V_2O_5, 99.3%, SHOWA) and titanium isopropoxide ($Ti(OCH(CH_3)_2)_4$, 97 %, ALDRICH). Lithium acetate was dissolved in ethanol and vanadium oxide was added. The titanium isopropoxide / isopropanol ($(CH_3)_2CHOH$, 99 %, ALDRICH) solution was then added. After stirring for 20 min, the solution was set, allowing to gel and then aging for 2 days to form the set-gels. The as-prepared wet gels were dried and followed by calcination at 800 °C for 12 hours under N_2 gas, separately, to prepare $Li_4Ti_{5-x}V_xO_{12}$, x = 0, 0.06, 0.12, 0.18, 0.24, 0.30, and were abbreviated with LTO, LTOV06, LTOV12, LTOV18, LTOV24 and LTOV30, respectively.

2.2. Cell fabrication

For the electrode fabrication, the active material i.e. the LTOV prepared, was mixed with acetylene carbon black (DENKA HS-100) and polyvinylidene fluoride in the weight ratio of 80 : 10 : 10 in N-methyl-2pyrrolidinone. The slurry was casted on Cu foil by doctor blade and dried at 80 °C in vacuum oven to form the electrode. Lithium foils were used as the counter and reference electrodes. 1M $LiPF_6$ in a mixture of ethylene carbonate (EC)-propylene carbonate (PC)-diethyl carbonate (DEC) with a volume ratio EC-PC-DEC = 1: 1: 1 as the electrolyte and Celgard 2400 polypropylene as the separator. The electrochemical properties were studied in the half-cell with CR2032 coin cells assembled in an argon-filled glove box, where the H_2O and O_2 concentrations were less than 1 ppm.

2.3. Characterization

The crystalline structures of the samples prepared were characterized on a PANalytical X'Pert Pro MRD X-ray diffraction spectroscopy (XRD) with Cu Kα radiation source (λ = 1.5418 Å). The element compositions of metals in the samples were determined by inductively coupled plasma optical emission spectrometer (ICP-OES, Agilent 725). The electronic conductivity measurements were performed with a four-point probe connected to a Keithley 2400 voltmeter constant-current source system. The X-Ray photoelectron spectroscopy (XPS) measurements were performed on Perkin Elmer PHI 5900. Nitrogen adsorption/desorption isotherms were determined on Micromeritics Tristar 3000. The scanning electron microscopy (SEM) images of samples were obtained at two magnifications (20kX and 100kX) using JEOL JEM-7600F. The transmission electron microscopy (TEM) and high resolution transmission electron microscopy (HRTEM) images of the samples were taken by JEOL JEM2000FX Ⅱ and JEOL JEM2100, respectively.

Both the cyclic voltammetry (CV) and electrochemical impedance spectroscopy (EIS) measurements were performed on AUTOLAB PGSTAT30. The cyclic voltammetry data was collected in the range of 1 - 2.5 V *vs.* Li/Li^+ at the various scan rates of 1, 2 and 5 mV s^{-1}. The EIS data was collected by applying AC amplitude of 5 mV over the frequency range of 10^5 - 10^{-2} Hz. Both the rate capability and galvanostatic charge-discharge cycling tests were performed on Land CT2001A (5 V, 2 mA) in the range of 1 - 2.5 V or 0 - 2.5 V. The C-rate was calculated from the weight and theoretical capacity of the LTO and LTOV electrodes. (1C = 175 mA g^{-1})

3. Results and discussion

3.1. Characterization of the $Li_4Ti_{5-x}V_xO_{12}$ samples

The element compositions of metals in LTOVs were measured by ICP-OES and the data are listed in Table 2. As expected, with increasing the amount of V_2O_5 the V concentration was increased and Ti concentration was decreased in LTOVs due to decrease the organic precursor (titanium isopropoxide) used.

Fig. 1a shows the XRD patterns of LTOVs with different vanadium contents (x) synthesized. As is observed, the main diffraction patterns of all the samples are the same and according to JCPDS card No-26-1198 the pattern is indexed to *Fd3m* space of the cubic spinel structured $Li_4Ti_5O_{12}$.[12] Unlike the $Li_4Ti_{5-x}V_xO_{12}$ prepared by the solid state method reported,[21] in which VO_2 phase was found in those with $x \geq 0.15$, only very weak peaks at $2\theta = 25.5^0$ and 27.5^0 for the anatase structure TiO_2 are observed in LTO, which was formed due to loss of the Li ion calcination at 800 °C.[25] However, the anatase phase was significantly diminished and no V-based phase was found. Besides, as indicated by the perpendicular dash lines, the shifts of the diffraction peak positions of the cubic spinel structures from that of pure LTO are negligible for all the LTOVs. This implies that the vanadium ions successfully replaced the titanium ions by the sol-gel method applied. The lattice parameters calculated from the XRD patterns using a Jade program according to the Rietveld method are listed in Table 2. The various lattice change of LTOVs after annealing are believed to be influenced by (1) the oxygen defect concentration under the heat treatment in nitrogen atmosphere[26] (2) the smaller ionic radii of vanadium ions (0.54 and 0.58 Å for V^{5+} and V^{4+}, respectively, while 0.605 and 0.67 Å for Ti^{4+} and Ti^{3+}, respectively)[27] and (3) the valence transition from Ti^{4+} to Ti^{3+} by charge compensation[14, 28, 29] as evidenced by XPS discussed below. Since these factors do not have the same trend as the vanadium concentration is increased, there is no trend for the lattice parameters resulted by the combination of these factors. Nevertheless, most of the lattice parameters of LTOVs were slightly smaller than that of the pure LTO (< 0.18 %) may be mainly ascribed to the smaller radii of the vanadium ions doped.

The oxidation states of the titanium and the vanadium in LTOVs were investigated by the XPS measurement and the Ti $2p_{3/2}$ and V $2p_{3/2}$ XPS curves of LTO, LTOV06 and LTOV18 measured are shown in Fig. 2 as the representatives. Besides, the spectra were deconvoluted by using the XPSPEAK program and the

corresponding analysis data are listed in Table 2. As shown in Fig. 2a-2c for the Ti $2p_{3/2}$ XPS spectra, the deconvoluted binding energy peak located at about 458.7 and 457.3 eV is assigned to Ti^{4+} and Ti^{3+}, respectively.[30] As listed in Table 2, no Ti^{4+} was reduced to Ti^{3+} in LTO and the Ti^{3+} content of LTOVs was increased from LTOV06 to LTOV18 then decreased for LTOV24 and LTOV30. On the other hand, although relatively low intensities of the peaks are found in the V $2p_{3/2}$ XPS spectra due to the low V-doping amount, the deconvoluted binding energy peaks located at around 517.3 and 516.2 eV,[30] corresponding to V^{5+} and V^{4+}, respectively, are seen in Fig. 2b' and 2c'. Fig. 2b' shows 100 % of the V^{4+} oxidation state in LTOV06 due to the lower V-doping amount, while only part of the V^{5+} was reduced to V^{4+} in LTOV18 as observed in Fig. 2c'. It confirms that the mixed valence of Ti^{4+} and Ti^{3+} as well as V^{5+} and V^{4+} were occurred due to the change in electronic structure and oxygen defect concentration under the heat treatment in nitrogen atmosphere.[26, 28] Since the electrochemical properties of the LTOV materials are related to their bulk electronic conductivities,[11, 14] which could be increased with increasing the percentage of the reduced forms of vanadium and titanium ions, therefore, it was anticipated that the best electrochemical properties would be obtained from LTOV06.

3.2. Electronic conductivity and textural properties of the $Li_4Ti_{5-x}V_xO_{12}$ samples

The electronic conductivities of LTOVs were investigated by the four-point probe DC method and the data is listed in Table 2. It clearly indicates that the highest electronic conductivity (4.512×10^{-8} S cm^{-1}) was obtained from LTOV06 and was about 35 % higher than that of LTO (3.349×10^{-8} S cm^{-1}).

The textural properties of LTOVs were measured by the nitrogen adsorption/desorption isotherms and listed in Table 2. As usually occurred in the samples synthesized by sol-gel process, the pores were formed in LTO and LTOVs prepared in this study. As shown in Fig. 3 the pore size distribution of LTO is peaked at 2.3 nm and the average pore size and the total pore volume is 13.85 nm and 0.010 cm^3 g^{-1}, respectively. The average pore diameter and total pore volumes of LTOV06 - LTOV18 were all higher than that of LTO and increased to about 25.64 - 28.63 nm and 0.011 - 0.018 cm^3 g^{-1}, respectively. These increases are believed to benefit the penetration of the electrolyte, resulting in a decrease in the resistance of the Li ion migration at the electrode/electrolyte interface.[31] However, the large decrease in total pore volume for LTOV24 and LTOV30 decreased the Li ion migration opportunity between the electrode and the electrolyte, leading to higher resistance.

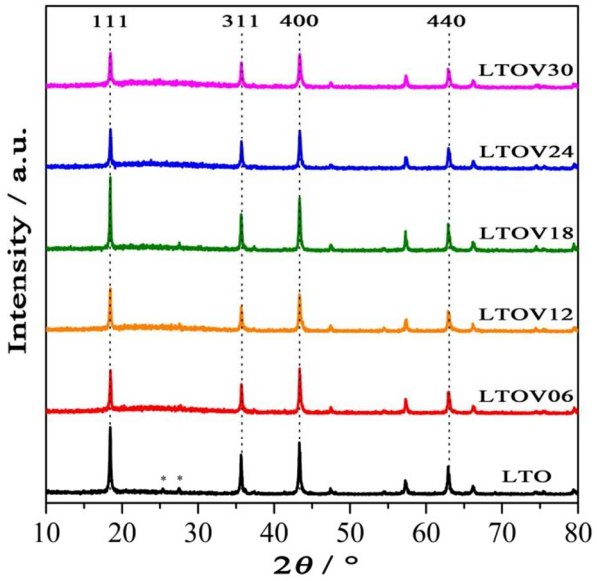

Fig. 1 XRD patterns of the $Li_4Ti_{5-x}V_xO_{12}$ samples.

Table 2 Element composition, lattice parameter, oxidation states and textural properties for the $Li_4Ti_{5-x}V_xO_{12}$ samples.

	LTO	LTOV06	LTOV12	LTOV18	LTOV24	LTOV30
Element composition						
Li / wt.%	6.03	6.04	6.04	6.04	6.03	6.02
Ti / wt. %	52.31	51.63	50.90	50.34	49.69	49.08
V / wt.%	-	0.64	1.37	1.93	2.55	3.20
Lattice parameter						
a / Å	8.3317	8.3190	8.3211	8.3386	8.3172	8.3163
Electronic conductivity						
κ / 10^{-8} S cm^{-1}	3.349	4.512	3.227	3.773	3.083	2.993
Oxidation state of Ti						
Ti^{4+} $2p_{3/2}$	100 %	90 %	92 %	83 %	90 %	96 %
Ti^{3+} $2p_{3/2}$	0 %	10 %	8 %	17 %	10 %	4 %
Oxidation state of V						
V^{5+} $2p_{3/2}$	-	0 %	69 %	59 %	67 %	78 %
V^{4+} $2p_{3/2}$	-	100 %	31 %	41 %	33 %	22 %
Textural properties						
Surface area / m^2 g^{-1}	3.69	2.30	1.68	2.33	0.39	0.42
Total pore volume / cm^3 g^{-1}	0.010	0.017	0.011	0.018	0.003	0.003
Average pore diameter / nm	13.85	25.64	26.66	28.63	52.23	49.06

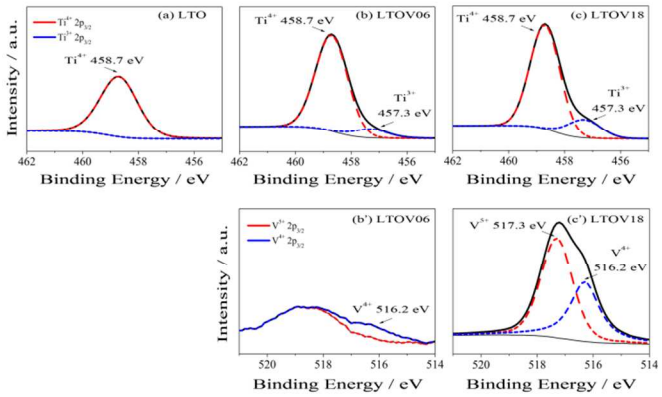

Fig. 2 XPS spectra of the $Li_4Ti_{5-x}V_xO_{12}$ samples. (a - c) Ti $2p_{3/2}$; (b' - c') V $2p_{3/2}$.

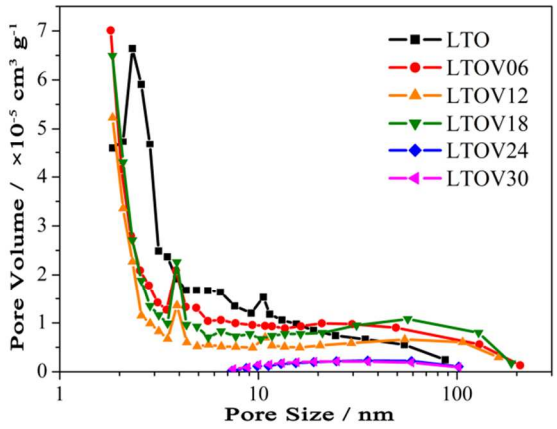

Fig. 3 Pore size distributions of the $Li_4Ti_{5-x}V_xO_{12}$ samples

3.3. Morphologies of the $Li_4Ti_{5-x}V_xO_{12}$ samples

The SEM images of LTOVs with different vanadium contents are depicted in Fig. 4 at two magnifications (20kX and 100kX). The high magnification images (a - f) demonstrate that as commonly found in the materials prepared by the sol-gel method the micron-particles in all the samples were formed by the nano-particles (5 - 15 nm).[7] In the low magnification images (a' - f'), it is observed that the chunks were clumped by the micron-particles and evenly coated with the carbon layer formed from the calcination of the organic precursors, lithium acetate and titanium isopropoxide, in the inert gas. The micron-particles in LTO and LTOV06 - LTOV18 were in the sizes of 0.3 - 1.5 μm and formed pores, while the larger micron-particles, ranged between 2 - 3 μm, were found in LTOV24 and LTOV30, resulting in the incomplete carbon layer and less pores. This reveals that for LTO and LTOV06 - LTOV18, the smaller micron-particles provided shorter Li ion diffusion distances,[23, 32] the evenly coated carbon layer enhanced the electron transport speed and more pores offered more active sites for the Li ions insertion/desertion process than for LTOV24 and LTOV30. That is the porous structures of LTO and LTOV06 - LTOV18 benefit the penetration of the electrolyte, profiting the Li ion migration at the electrode/electrolyte interface and the smaller micron-particles in LTO and LTOV06 - LTOV18 effectively shorten the diffusion distance for the Li ion in the center of particle to the surface, accelerating the Li ion movement in the bulk, consequently increasing the electronic conductivity. These results not only agree with their textural properties but also support that the electronic conductivities of LTO and LTOV06 - LTOV18 were higher than that of LTOV24 and LTOV30 as mentioned above and anticipated to have better performance.

The TEM image of LTO is shown in Fig. 5a. It exhibits that LTO is composed of the primary particles with size of 5 - 15 nm and is in agreement with the SEM result. The high-resolution transmission electron microscopy energy dispersion spectroscopy (HRTEM-EDS) mapping for LTOV06 is depicted in Fig. 5b-5c. As can been seen, the Ti and V were uniformly distributed in the sample. The TEM image in Fig. 5d shows that the lattice space of LTVO06 is 0.48 nm, corresponding to the lattice spaces (111) planes of spinel $Li_4Ti_5O_{12}$. The lattice fringe indicates well-crystallinity of the nanoparticles in LTOV06. Besides, the SAED pattern of LTOV06 depicted in Fig. 5e shows a well-resolved concentric rings with bright spots, corresponding to the (111), (220), (311), (400) and (440) diffraction planes of the spinel $Li_4Ti_5O_{12}$ and indicating that the particles are polycrystalline, which is in good agreement with the XRD result.

3.4. Cyclic voltammetry performance of the $Li_4Ti_{5-x}V_xO_{12}$ electrodes

The electrochemical properties of all the LTOV electrodes were investigated by the coin cells with half-cell configurations. The cyclic voltammograms (CVs) between 1 and 2.5 V *vs.* Li/Li^+ measured with a scan rate of 1 mV s^{-1} are shown in Fig. 6a. As can be seen, the CVs of all the electrodes are similar, suggesting that the V-doping only slightly affected the electrochemical reactions. The anodic (oxidation) potential peaked at about 1.78 - 1.81 V and the cathodic (reduction) potential peaked at about 1.49 - 1.53 V correspond to the Li ions desertion and insertion process in the electrode, respectively. The higher current densities for the LTO and LTOV06 electrodes than for the others reveal that the electrochemical activities were higher in these two electrodes. Fig. 6b shows the CVs of the LTO and LTOV06 electrodes scanned with various rates. It indicates that the CV curves were broadened with increasing the scan rate and the current density of the LTOV06 electrode was slightly higher than that of the LTO electrode at all the scanning rates, suggesting that the electrochemical activity of the LTOV06 electrode was slightly better than that of the LTO electrode due to the V-doping. This is consistent with the electronic conductivities discussed above.

3.5. Rate capability and galvanostatic charge-discharge capacity of the $Li_4Ti_{5-x}V_xO_{12}$ electrodes

The rate capabilities of the LTOV electrodes in the voltage range of 1 - 2.5 V at rates between 0.2 and 5 C are shown in Fig. 7. The discharge capacities of the pristine LTO electrode

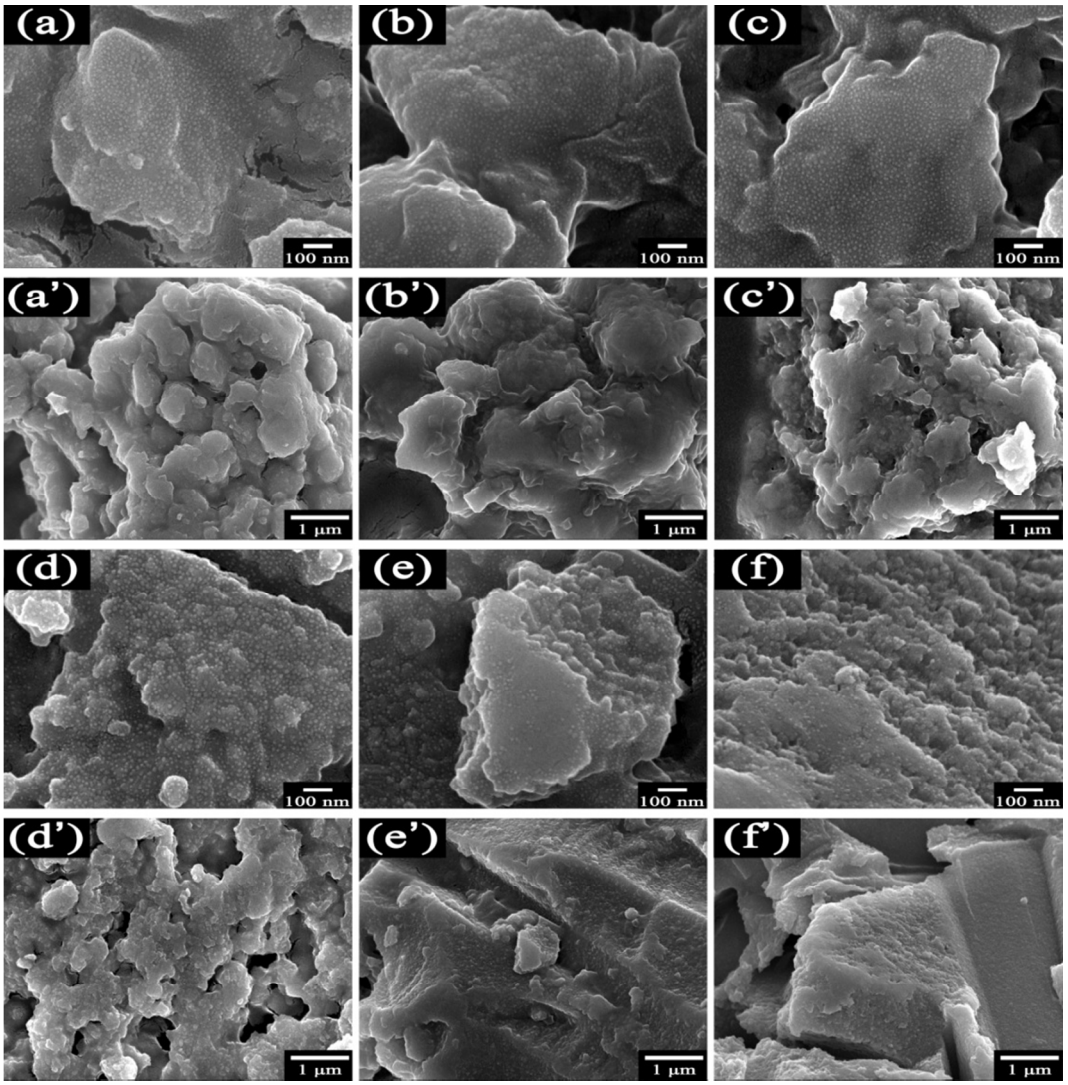

Fig. 4 SEM images of the $Li_4Ti_{5-x}V_xO_{12}$ samples. (a) LTO, (b) LTOV06, (c) LTOV12, (d) LTOV18, (e) LTOV24 and (f) LTOV30 at 100kX magnification. (a') LTO, (b') LTOV06, (c') LTOV12, (d') LTOV18, (e') LTOV24 and (f') LTOV30 at 20kX magnification.

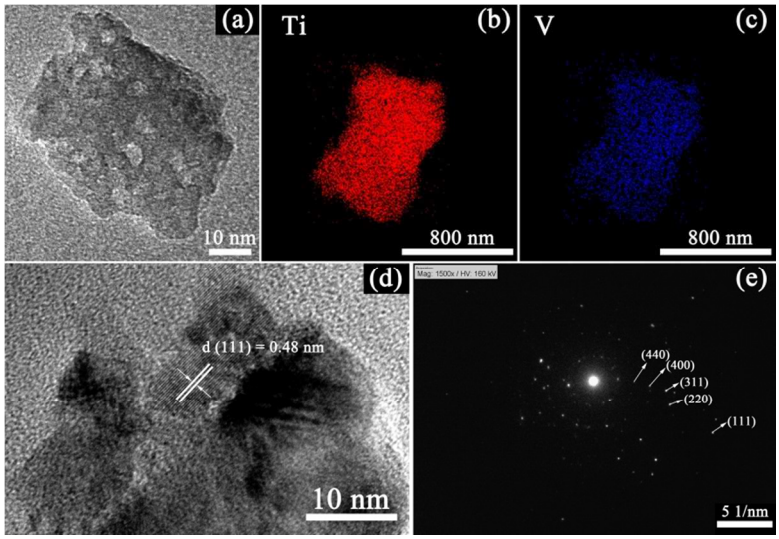

Fig. 5. (a) TEM image of LTO; TEM-EDS element mapping of LTOV06. (b) Ti, (c) V; (d)TEM image and (e) SAED pattern of LTOV06.

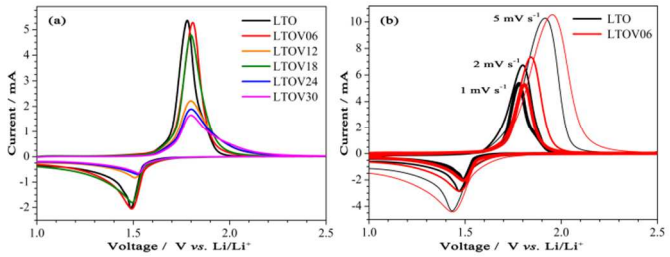

Fig. 6 Cyclic voltammogram properties in the voltage of 1 - 2.5 V for : (a) the $Li_4Ti_{5-x}V_xO_{12}$ electrodes at a scan rate of 1 mV s^{-1}; (b) the LTO and LTOV06 electrodes at various scan rates.

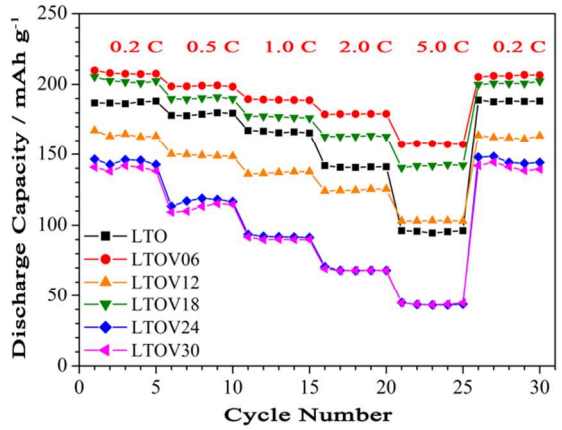

Fig. 7 Rate capabilities of the $Li_4Ti_{5-x}V_xO_{12}$ electrodes at various rates between 0.2 and 5 C in 1- 2.5 V.

obtained were 188 (0.2 C), 180 (0.5 C), 166 (1 C), 141 (2 C) and 96 mAh g^{-1} (5 C). The capacity at 0.2 C was slightly higher than the theoretical value of 175 mAh g^{-1} and that prepared with the solid state method (167 mAh g^{-1}).[21] This is mainly ascribed to the presence of the nano-particles formed by the sol-gel process, resulting in an increase in the contact area with the electrolyte, and the smaller micron-particles that shortened the Li-ions diffusion distance.[11] Besides, the discharge capacities of the LTOV06 and LTOV18 electrodes (208 and 202 mAh g^{-1} at 0.2 C, respectively) were higher than that of the pristine LTO electrode due to increase of the Ti^{3+} content by V doping. At 5 C, the capacity of the LTO, LTOV06 and LTOV18 electrodes was 92, 157 and 146 mAh g^{-1}, respectively. However, the capacities of the LTOV12 electrode at the rates between 0.2 and 2 C were lower than that of the LTO, LTOV06 and LTOV18 electrodes but slightly higher than that of the LTO electrode at 5 C. The results suggest that the capacity of the LTOV electrode not only depends on the morphology of the materials but also the combination of the Ti^{3+}/Ti^{4+} and V^{4+}/V^{5+} ratios because higher percentages of Ti^{3+} and V^{4+} may benefit to the electronic conductivity.[14] Similarly, the lower capacities for the LTOV24 and LTOV30 electrodes can be attributed to the lower percentage of Ti^{3+} and V^{4+}, the larger particle size and the incomplete carbon coating. Nevertheless, they exhibited better rate capability than that prepared with high-speed ball milled method.[11]

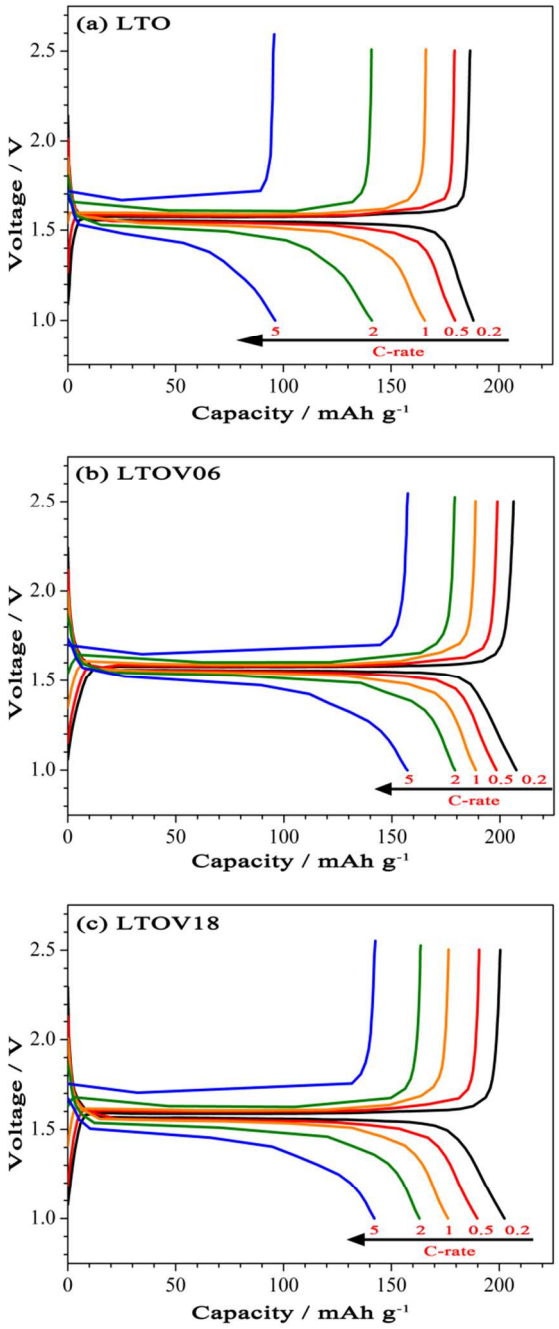

Fig. 8 Charge-discharge curves of the $Li_4Ti_{5-x}V_xO_{12}$ electrodes: (a) LTO, (b) LTOV06, (c) LTOV18, at various rates between 0.2 and 5 C in 1- 2.5 V.

In addition, it is also found that all the capacities of the LTOV electrodes re-measured at 0.2 C after the high-rate capability tests were all similar to the corresponding initial capacities measured at 0.2 C, confirming the zero-strain of LTOVs in the cubic lattice that lead to the good capacity retention even at high-rate.

Fig. 8 shows the charge-discharge curves of rate capabilities for the LTO, LTOV06 and LTOV18 electrodes at various rates between 0.2 and 5 C. At 0.2 C the discharge plateaus appear at ~1.55 V *vs.* Li/Li^+, corresponding to the

redox of Ti^{4+}/Ti^{3+} for the LTO, LTOV06 and LTOV18 electrodes. Besides, the potential difference between charge and discharge platform increased with increasing the rate, i.e. increased the electrode polarization, implying that less Li ions could insert into and desert out of the LTOV electrodes at high-rate. However, compared to that for the pristine LTO electrode, the electrode polarization is smaller for the LTOV06 and LTOV18 electrodes, especially at high-rate, indicating that the V-doping not only increased the capacity but also decreased the electrode polarization for the LTOV electrodes at high-rate.

The cyclic performances of the $Li_4Ti_{5-x}V_xO_{12}$ electrodes at 1 C in the range of 1 - 2.5 V are shown in Fig. 9a. As can be seen, good capacity retention was obtained for all the electrodes. This is ascribed to the zero-strain of the cubic lattice. The fact that some capacities were slightly higher than the initial capacity is ascribed to that the electrolyte was better penetrated into the electrode after several charge-discharge cycles. For comparison with some of the results reported,[15, 17-19, 22] the electrochemical behaviors of the LTO, LTOV06 and LTOV18 electrodes at lower voltage (0 - 2.5 V) were studied as well and the cyclic performances at 5 C are shown in Fig. 9b. It shows that the initial capacity of the LTO and LTOV06 electrode were 301 and 243 mAh g^{-1}, respectively, and the capacity of the 250th cycle were 230 and 216 mAh g^{-1}, respectively. Although the capacities of the LTOV06 electrode in this range were all lower than that of the pristine LTO electrode in the cyclic tests, its high capacity retention of 89 % after 250 cycles was much higher than that of 76 % and 67 % for the pristine LTO and LTOV18 electrodes. This less irreversible capacity for LTOV06 implies that when discharge to 0 V, less solid electrolyte interface (SEI) layer was formed on the LTOV06 electrode than the LTO and LTOV18 electrodes.[12, 22]

3.6. Electrochemical impedance spectroscopy

Fig. 10 shows the Nyquist plots of the LTO and LTOV06 electrodes and the equivalent circuit in the inset. The electrochemical impedance spectroscopy (EIS) results were fitted by the selected equivalent circuit using a ZView program and the corresponding impedance parameters are listed in Table 3. It shows that all the plots are comprised of a depressed semicircle in the high to medium frequency regions and a straight line in the low frequency region. The plot in the high frequency intercepted at the real axis corresponds to the ohmic resistance of the cell mainly contributed from the electrolyte (R_s). The semicircle in the high to medium frequency region mainly represents the resistance in the migration of the Li ions at the electrode/electrolyte interface (R_{ct}) in parallel with a double-layer capacitance (CPE). The straight line in the low frequency region is attributed to the diffusion of the Li ions into the bulk of the electrode material, which is called Warburg diffusion (Z_w).[11, 33] Table 3 indicates that the R_s values of the LTO and LTOV06 electrodes are similar, but the R_{ct} value of the LTOV06 electrode was about two times lower than that of the LTO electrode, revealing that the migration of the Li ions at the electrode/electrolyte interface was easier in the LTOV06 electrode. Moreover, EIS result can be used to calculate the Warburg impedance coefficient (σ_w) from Eq. (1) and the Li diffusion coefficient (D_{Li}) of the Li ions diffusing into the electrode materials from Eq. (2)[34]

$$Z_{re} = R_s + R_{ct} + \sigma_w \omega^{-1/2} \quad (1)$$

$$D_{Li} = R^2T^2 / 2A^2n^4F^4C^2\sigma_w^2 \quad (2)$$

where Z_{re} is the real resistance of the cell, ω is the angular frequency, R is the gas constant, T is the absolute temperature, A is the surface area of the electrode, n is the number of electrons transferred in the half-reaction for the redox couple, F is the Faraday constant, C is the concentration of Li ion in solid (4.37×10^{-3} mol cm^{-3}).[35]

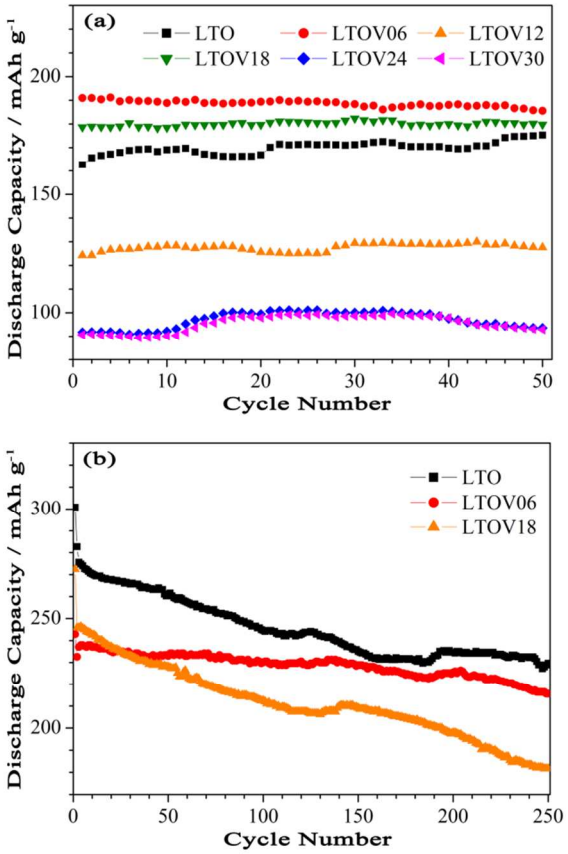

Fig. 9 Cyclic performances for the $Li_4Ti_{5-x}V_xO_{12}$ electrodes: (a) at 1 C in 1 - 2.5 V; (b) at 5 C in 0 - 2.5 V.

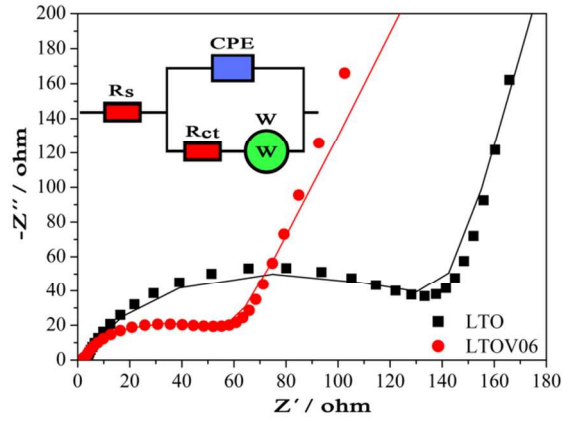

Fig. 10 Nyquist plots of the LTO and LTOV06 electrodes and equivalent circuit inset.

Table 3 Impedance parameters derived using equivalent circuit model of the LTO and LTOV06 electrodes

Sample	R_s (Ω)	R_{ct} (Ω)	σ_w (Ω cm^2 s$^{-1/2}$)	D_{Li} (cm^2 s^{-1})
LTO	3.02	120.5	119.32	2.11×10^{-13}
LTOV06	1.82	60.4	109.14	2.53×10^{-13}

As listed in Table 3, the σ_w value of the LTOV06 electrode was lower than that of the LTO electrode, implying that Li ions diffused in the LTOV06 electrode faster than in the LTO electrode. As the result, the R_{ct} and σ_w values of the LTOV06 electrode were significantly lower than that of the LTO electrode, leading to the better electronic and ionic conductivity. This result is consistent with the conductivity result discussed above.

4. Conclusions

In this study, a series of the spinel-type vanadium-doped $Li_4Ti_{5-x}V_xO_{12}$ ($0 \leq x \leq 0.3$) (LTOVs) samples were successfully synthesized by the sol-gel method. It was found that the doping of V ions in the Ti sites of LTO did not change the original spinel-type structure while increased the ratio of Ti^{3+} and Ti^{4+} oxidation states that benefited the electron transport. The electronic conductivity of LTOV06 (4.512×10^{-8} S cm^{-1}) was higher than that of the other $Li_4Ti_{5-x}V_xO_{12}$ samples, which enhanced the electrochemical activity. The SEM images revealed formation of the nano-particles (5 - 15 nm) by the sol-gel process that favored the electrochemical properties. Compared to the other electrodes prepared, the LTOV06 electrode exhibited the best electrochemical properties in rate capability and cyclic performance in the voltage range of 1 - 2.5 V at the various rates between 0.2 C (208 mAh g^{-1}) and 5 C (157 mAh g^{-1}). Besides, in the voltage range of 0 - 2.5 V at 5 C, the initial capacity of the LTOV06 electrode was as high as 243 mAh g^{-1} and its capacity retention was 89 % after 250 cycles. The results indicate that LTOV06 prepared is the best V-doping LTO electrode materials reported up to now and is promising as a high-rate anode material for power lithium ion batteries.

Acknowledgements

The authors gratefully acknowledge the Ministry of Science and Technology, Taiwan, R.O.C. for supporting this research work under grant number: NSC 103-2113-M-033-002-MY3.

Notes

[a]*Department of Chemistry,* [b]*Center for Nanotechnology,* [c]*Center for Biomedical Technology, Chung Yuan Christian University, 200 Chung-Pei Rd., Chung-Li District, Tao-Yuan City, Taiwan 32023, R.O.C.*

E-mail: yuiwhei@cycu.edu.tw (Yui Whei Chen-Yang); Tel.: +886 3 265 3317; Fax: +886 3 265 3399.

References

1. N. Takami, H. Inagaki, Y. Tatebayashi, H. Saruwatari, K. Honda and S. Egusa, *J. Power Sources*, 2013, **244**, 469-475.
2. G. P. Hammond and T. Hazeldine, *Applied Energy*, 2015, **138**, 559-571.
3. M. Hu, X. Pang and Z. Zhou, *J. Power Sources*, 2013, **237**, 229-242.
4. K. Ariyoshi, R. Yamato and T. Ohzuku, *Electrochim. Acta*, 2005, **51**, 1125-1129.
5. K. Zaghib, A. Mauger, H. Groult, J. Goodenough and C. Julien, *Materials*, 2013, **6**, 1028-1049.
6. B. Tian, H. Xiang, L. Zhang, Z. Li and H. Wang, *Electrochim. Acta*, 2010, **55**, 5453-5458.
7. Y. Wu, M. V. Reddy, B. V. R. Chowdari and S. Ramakrishna, *Electrochim. Acta*, 2012, **67**, 33-40.
8. H. Li, L. Shen, X. Zhang, J. Wang, P. Nie, Q. Che and B. Ding, *J. Power Sources*, 2013, **221**, 122-127.
9. T.-F. Yi, L.-J. Jiang, J. Shu, C.-B. Yue, R.-S. Zhu and H.-B. Qiao, *J. Phys. Chem. Solids* 2010, **71**, 1236-1242.
10. A. Guerfi, P. Charest, K. Kinoshita, M. Perrier and K. Zaghib, *J. Power Sources*, 2004, **126**, 163-168.
11. Z. Yu, X. Zhang, G. Yang, J. Liu, J. Wang, R. Wang and J. Zhang, *Electrochim. Acta*, 2011, **56**, 8611-8617.
12. J.-Y. Lin, C.-C. Hsu, H.-P. Ho and S.-H. Wu, *Electrochim. Acta*, 2013, **87**, 126-132.
13. Z. Wang, G. Chen, J. Xu, Z. Lv and W. Yang, *J. Phys. Chem. Solids*, 2011, **72**, 773-778.
14. R. Cai, S. Jiang, X. Yu, B. Zhao, H. Wang and Z. Shao, *J. Mater. Chem.*, 2012, **22**, 8013-8021.
15. S. Huang, Z. Wen, X. Zhu and Z. Lin, *J. Electrochem. Soc.*, 2005, **152**, A186-A190.
16. X. Li, M. Qu and Z. Yu, *J. Alloys Compd.*, 2009, **487**, L12-L17.
17. T.-F. Yi, Y. Xie, L.-J. Jiang, J. Shu, C.-B. Yue, A.-N. Zhou and M.-F. Ye, *RSC Adv.*, 2012, **2**, 3541-3547.
18. Y.-R. Jhan and J.-G. Duh, *Electrochim. Acta*, 2012, **63**, 9-15.
19. T.-F. Yi, Y. Xie, Q. Wu, H. Liu, L. Jiang, M. Ye and R. Zhu, *J. Power Sources*, 2012, **214**, 220-226.
20. W. Long, X. Wang, S. Yang, H. Shu, Q. Wu, Y. Bai and L. Bai, *Mater. Chem. Phys.*, 2011, **131**, 431-435.
21. T.-F. Yi, J. Shu, Y.-R. Zhu, X.-D. Zhu, C.-B. Yue, A.-N. Zhou and R.-S. Zhu, *Electrochim. Acta*, 2009, **54**, 7464-7470.
22. T.-F. Yi, J. Shu, Y.-R. Zhu, X.-D. Zhu, R.-S. Zhu and A.-N. Zhou, *J. Power Sources*, 2010, **195**, 285-288.
23. A. Mahmoud, J. M. Amarilla, K. Lasri and I. Saadoune, *Electrochim. Acta*, 2013, **93**, 163-172.
24. P. Kubiak, A. Garcia, M. Womes, L. Aldon, J. Olivier-Fourcade, P.-E. Lippens and J.-C. Jumas, *J. Power Sources*, 2003, **119-121**, 626-630.
25. C.-m. Shen, X.-g. Zhang, Y.-k. Zhou and H.-l. Li, *Mater. Chem. Phys.*, 2002, **78**, 437-441.
26. X. Chen, X. Guan, L. Li and G. Li, *J. Power Sources*, 2012, **210**, 297-302.
27. R. D. Shannon, *Acta. Crystallogr. A*, 1976, **32**, 751-767.
28. H. Song, T. G. Jeong, Y. H. Moon, H. H. Chun, K. Y. Chung, H. S. Kim, B. W. Cho and Y. T. Kim, *Scientific reports*, 2014, **4**, 4350.
29. S.-K. Kim, E.-S. Kwon, T.-H. Kim, J. Moon and J. Kim, *Ceram. Int.*, 2014, **40**, 8869-8874.

30. C. D. Wagner, W. M. Riggs, L. E. Davies, J. F. Moulder and G. E. Muilenberg, *Handbook of X-ray Photoelectron Spectroscopy*, Perkin-Elmer, Eden Prairie, MN, 1979.
31. D. Shao, J. He, Y. Luo, W. Liu, X. Yu and Y. Fang, *J Solid State Electrochem*, 2012, **16**, 2047-2053.
32. Y. Shen, J. R. Eltzholtz and B. B. Iversen, *Chem. Mater.*, 2013, **25**, 5023-5030.
33. C. Lin, X. Fan, Y. Xin, F. Cheng, M. O. Lai, H. Zhou and L. Lu, *Nanoscale*, 2014, **6**, 6651-6660.
34. B. Jin, E. M. Jin, K.-H. Park and H.-B. Gu, *Electrochem. Commun.*, 2008, **10**, 1537-1540.
35. S.-L. Chou, J.-Z. Wang, H.-K. Liu and S.-X. Dou, *J. Phys. Chem. C*, 2011, **115**, 16220-16227.

